A new Organic–Inorganic hybrid compound (NH3(CH2)2C6H5)2[SnCl6]: Crystal structure, characterization, Hirshfeld surface analysis, DFT calculation, vibrational properties and biological evaluation

Abdellah Kaiba, Mohammed Geesi, Yassine Riadi, Elmutasim O. Ibnouf, Talal Aljohani, Philippe Guionneau

A New Organic–Inorganic Hybrid Compound $(NH_3(CH_2)_2C_6H_5)_2[SnCl_6]$: Crystal Structure, Characterization, Hirshfeld Surface Analysis, DFT Calculation, Vibrational Properties and Biological Evaluation

Abdellah. Kaiba[a], Mohammed H. Geesi[b], Yassine Riadi[c], Elmutasim O. Ibnouf[d,e], Talal A. Aljohani[f], Philippe. Guionneau[g],

[a]Department of Physics, College of Science and Humanities in Al-Kharj, Prince Sattam bin Abdulaziz University, Al-Kharj 11942, Saudi Arabia

[b]Department of Chemistry, College of Science and Humanities in Al-Kharj, Prince Sattam bin Abdulaziz University, Al-Kharj 11942, Saudi Arabia

[c]Department of Pharmaceutical Chemistry, College of Pharmacy, Prince Sattam bin Abdulaziz University, Al-Kharj 11942, Saudi Arabia.

[d]Department of Pharmaceutics, College of Pharmacy, Prince Sattam bin Abdulaziz University, Al-Kharj 11942, Saudi Arabia

[e]Department of Medical Microbiology, Faculty of Medical Laboratory Sciences, Omdurman Islamic University, Sudan

[f]King Abdulaziz City for Science and Technology, Riyadh, Saudi Arabia

[g]CNRS, Univ. Bordeaux, Bordeaux INP, ICMCB, UMR 5026, 87 av. Dr A. Schweitzer, F-33600 Pessac (France)

Abstract

In this study, the crystal structure of a new phase of organic–inorganic hybrid $(NH_3(CH_2)_2C_6H_5)_2[SnCl_6]$ was resolved at room temperature (monoclinic system), space group (P21/c), with unit cell parameters (***a*** = 7.345(5) Å, ***b*** = 25.667(5) Å, ***c*** = 11.971(5) Å), β = 90.106(5)°, volume = 2256.8 (19) $Å^3$ and ***Z*** = 4). The asymmetric unit cell consisted of a combination of $[SnCl_6]^{2-}$ and two organic $^+NH_3C_2H_4C_6H_5$ cations. The crystal structure comprised alternating organic and inorganic layers stacked along the *b*-axis. The isolated octahedra formed a zero-dimensional anionic network. The crystal structure was stabilized by hydrogen bonding. Powder X-ray diffraction confirmed the phase purity. Hirshfeld surface and fingerprint plots elucidated the contribution of the H···Cl and H···H intermolecular interactions. DFT calculations confirmed the assignment of the Raman bands. Vibrational absorption bands were identified by micro-Raman spectroscopy. The antibacterial performance was investigated. Notably, this new compound was active against all of the tested bacteria.

Keywords: X-ray diffraction, Hirshfeld surface, DFT calculation, Micro-Raman spectroscopy, Antibacterial

*Corresponding author:

E-mail address: a.kaiba@psau.edu.sa (A. Kaiba)

Address: Department of Physics, College of Science and Humanities in Al-Kharj, Prince Sattam bin Abdulaziz University, Al-Kharj 11942, Saudi Arabia

1. Introduction

In recent years, organic–inorganic hybrids have become one of the most attractive research topics due to the possibility of integrating the advantageous properties of inorganic and organic molecules, including electrical, optical, magnetic and catalytic properties, as well as luminescence and conductivity. The selection of metals such as Tin (Sn)in medicine for example poses a key issue in terms of its toxicity in comparison with that of lead (Pb) [1-6]. Owing to their interesting structures, these composites have been intensely studied to better correlate their structure with physical properties [7-9]. These compounds exhibit a perovskite-type structure, where the inorganic layer is composed of an MX_6 octahedra or tetrahedral MX_4. The cohesion between the interlayers in such compounds in the solid state generally occurs by hydrogen bonding, π-stacking, π–π stacking and van der Waals interactions [10-13]. Furthermore, some hybrids of this family exhibit the highest energy conversion efficiency for photovoltaic cells [14-20]. This perovskite sub-family is a fascinating family of functional materials, particularly perovskite based on stannate halide, due to its numerous attractive properties, including photoluminescence, optical, electrical and catalytic properties [21-23].

In addition, interesting aspects of the inorganic and organic chemistry of tin have been discussed in various reviews [24]; these derivatives have attracted considerable attention due to their interesting optical properties [22, 23], the development of cost-effective electronic devices [22], agriculture, medicine, anti-fouling paints and biological activities [25-28].

In this study, phenethylamine ($C_8H_{11}N$) ligand and tin(II) chloride were used as the organic and inorganic parts, respectively, for the preparation of the $(NH_3\text{-}(CH_2)_2\text{-}C_6H_5)_2[SnCl_6]$ compound. In this study, the main aim was to synthesize a new phase of the $(NH_3\text{-}(CH_2)_2\text{-}C_6H_5)_2[SnCl_6]$ compound, examine its crystal structure and characterize it by spectroscopic techniques. Hirshfeld surface analysis allowed the examination the network of interactions, and density functional theory (DFT) calculations allowed the structure optimization and the vibrational modes attributions. The calculated vibrational spectra were compared to the experimental spectrum to assign the vibration modes and to provide deep insights into the characteristic bonding within the structure. In addition, the antibacterial activity of the synthesized compound was investigated against four bacterial strains.

2. Experimental section

2.1 Synthesis of the title compound

Single crystals of $(NH_3\text{-}(CH_2)_2\text{-}C_6H_5)_2[SnCl_6]$ were obtained by mixing a aqueous solution of phenethylamine ($C_8H_{11}N$) protonated by Chloric acid (37% HCl, 1 mL) with aqueous solution of tin(II) chloride. A transparent homogeneous solution was formed. The single crystal suitable for single X-ray Diffraction (XRD) was obtained after several days by slow evaporation at room temperature.

2.2 Instrumental procedures

To examine the purity of the title compound, a K-Alpha XPS instrument (Thermo Fisher Scientific, United Kingdom) equipped with a micro-focused monochromatic Al Ka X-ray source (1486.6 eV) was employed for XPS analysis. A scanning electron microscopy SEM (model Quanta FEG 250, Netherlands) system was employed to observe the grain morphology of this compound. Vibrational modes were investigated on a SENTERRA II Compact Raman Microscope (Bruker, Germany) using a green laser with λ = 532 nm and a power of 0.25 mW in the range 50–4000 cm^{-1}. Powder

XRD patterns as a function of temperature were recorded on an Ultima IV X-ray diffractometer made in Japan operated in the θ–2θ Bragg–Brentano geometry [29] equipped with an X-ray source (Cu Kα).

2.3 Crystal structure

Single-crystal XRD patterns were recorded on a Nonius Kappa CCD diffractometer with a Mo anticathode. The ϕ and ω scan modes were utilized with a crystal-to-detector distance of 40 mm. The mosaicity degree of the selected crystal is about 0.35°. The structure was solved at room temperature. Data reduction was performed using the DENZO-SMN program. The SIR 97 program was employed to solve the structure [30]**,** and the SHELX 97 program was employed for the refinement of all atomic parameters by using the full-matrix least-squares technique based on the squared structure factor F^2[31]. Hydrogen atoms were theoretically located and isotropically refined. These programs were utilized within the WINGX package [32]. The DIAMOND [33] and MERCURY [34] programs were employed for all graphics. Table 1 summarizes the results from data measurements and refinement. In 2007, Billing et al. have reported another phase of this compound (system (monoclinic), space group ($P2_1/c$), unit cell parameters (***a*** = 12.243(2) Å, ***b*** = 7.1124(13) Å, ***c*** = 13.777(3) Å) and β = 93.697(3))[35]. Structural data can be obtained free of charge from the Cambridge crystallographic data centre (No: CCDC 2041258) at www.ccdc.cam.ac.uk/data_request/cif.

2.4 Minimum inhibitory concentration

The minimum inhibitory concentration (MIC) is referred to as the concentration of the derivative at which bacterial growth is completely inhibited. The MIC was determined by the double microdilution method with sterile flat-bottomed 96-well polystyrene plates, as detailed in reference [8].

Dimethyl sulfoxide (DMSO) was used as the negative control. The MIC was determined as follows: First, the compound was adjusted to concentrations of 100, 75, 50, 38.5, 25, 18.75 and 12.5 µg/mL in DMSO. Second, 200 µL of the old serially diluted test samples was dispensed into 96-well microtrays. Then, test bacteria were inoculated into the wells, the final volume was adjusted to 400 µL and the plates were incubated at 37°C for 24 h. The concentration at which a marked reduction in colour is observed is referred to as the MIC. All experiments were performed in triplicate.

2.5 Computational Details

The unit cell of the crystal structure was directly utilized as the initial molecular geometry of $(NH_3\text{-}(CH_2)_2\text{-}C_6H_5)_2[SnCl_6]$. Visualization and exploration of intermolecular contacts of a structure was achieved by Hirshfeld surface analysis [36] calculated by using Crystal Explorer software [37]. All calculations were performed using the Gaussian 16w package [38]. The Becke's three-parameter exchange functional combined with the Lee–Yang–Parr correlation functional (B3LYP) and LanL2DZ as the basis set were used for optimization and vibrational frequency calculations [39-43]. An empirical scaling factor of 0.961 [44] was utilized to offset the systematic error caused by basis set incompleteness, neglect of electron correlation and vibrational anharmonicity. The Gaussview 6.1.1 program [45] was utilized for visualization and presentation as well as the verification of the normal mode assignments.

Table 1: Crystal data and structure refinement details of $(NH_3\text{-}(CH_2)_2\text{-}C_6H_5)_2[SnCl_6]$.

Formula weight	575.76
Temperature	293(2) K
Wavelength	0.71069 Å
Crystal system	Monoclinic
Space group	P 2_1/c
Unit cell dimensions	a = 7.345(5) Å b = 25.667(5) Å β= 90.106(5)° c = 11.971(5) Å
Volume	2256.8(19) $Å^{-3}$
Z	4
Density (calculated)	1.695 Mg/m^3
Absorption coefficient	1.846 mm^{-1}
F(000)	1144
Crystal size	0.13 x 0.12 x 0.08 mm^3
Theta range for data collection	2.326 to 26.371°.
Index ranges	-9<=h<=9, -32<=k<=32, -14<=l<=14
Reflections collected	66918
Independent reflections	4593 [R(int) = 0.0470]
Completeness to theta = 25.24°	99.5 %
Refinement method	Full-matrix least-squares on F^2
Data / restraints / parameters	4593 / 14 / 217
Goodness-of-fit on F^2	1.298
Final R indices [I>2sigma(I)]	R1 = 0.0516, wR2 = 0.1164
R indices (all data)	R1 = 0.0528, wR2 = 0.1169
Largest diff. peak and hole	1.036 and -0.979 e. $Å^{-3}$

3 Results and Discussion

3-1 Powder x-ray diffraction at room temperature:

Powder XRD patterns as a function of temperature were recorded on an Ultima IV X-ray diffractometer operated in the θ–2θ Bragg–Brentano geometry equipped with an X-ray source (Cu Kα). The purity and crystallinity of the sample were examined by powder XRD. **Fig.1** shows the XRD pattern of the title material and the pattern simulated from its structure. Clearly, the powder and simulated diffractograms are superposed that explain that this phase is pure.

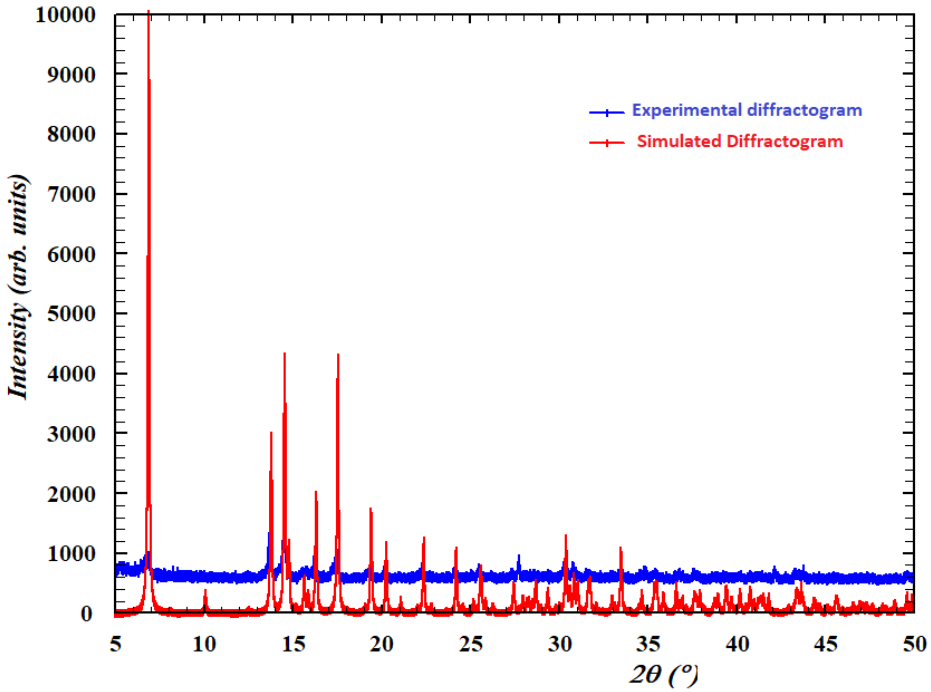

Figure1: Comparison of experimental and simulated X-ray diffraction patterns of $(NH_3\text{-}(CH_2)_2\text{-}C_6H_5)_2[SnCl_6]$

3-2 XPS analysis

The XPS survey scan (Fig 2) shows a characteristic peaks attributed to Carbon (C), tin (Sn), chloride (Cl), and nitrogen (N) atoms. The essential peaks are O_{1s}, Sn_{3d}, N_{1s}, C_{1s} and Cl_{2p} positioned at 533eV, 488 eV, 395eV, 277 eV and 200 eV respectively. The atomic percentage of Carbon atom is about 53.63% , of Nitrogen atom is about 4.91%, of Chlorine is about 13.51% of Tin atom is about 6.86%. Finally, the survey scan shows the presence of 21.09% of oxygen atom which is not present in the structure see XRD part (3.1 section). We believe that this oxygen comes from humidity.

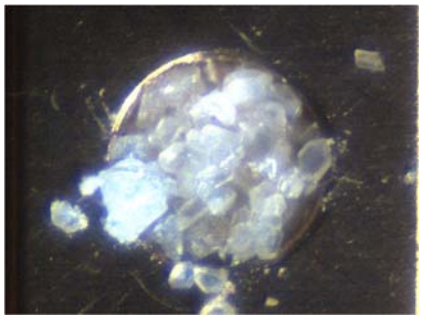

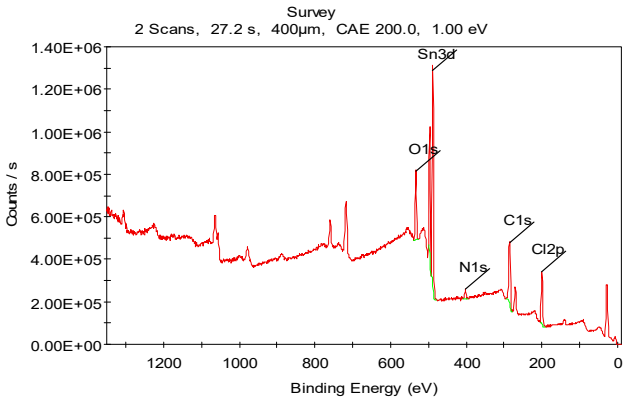

Figure 2: The whole XPS spectrum of $(NH_3\text{-}(CH_2)_2\text{-}C_6H_5)_2[SnCl_6]$.

3-3 Scanning Electron Microscopy

In the SEM micrograph of the $(NH_3\text{-}(CH_2)_2\text{-}C_6H_5)_2[SnCl_6]$ single crystal, a foliated-like structure, as well as enormous crystal fragments with a uniform distribution, and a smooth surface were observed, indicative of good crystallinity for this compound [46, 47], this result confirms the layered perovskite structure (Fig 3).

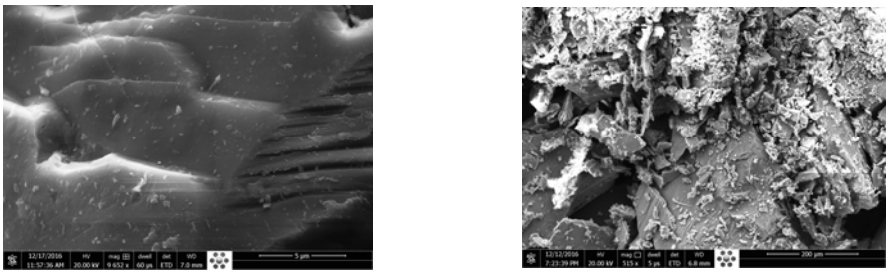

Figure.3: SEM micrographs of $(NH_3\text{-}(CH_2)_2\text{-}C_6H_5)_2[SnCl_6]$

3-4 Crystal structure determination

The prepared compound crystallized in a monoclinic system with the P 21/c space group and unit-cell dimensions of ***a*** = 7.345(5) Å, ***b*** = 25.667(5) Å, ***c*** = 11.971(5) Å, β = 90.106(5) and ***Z*** = 4 parameters. The asymmetric unit comprised two cations of $[C_6H_5\text{-}(CH_2)_2\text{-}NH_3]^+$ and an isolated hexachlorostannate anion of $[SnCl_6]^{2-}$ **(**Fig. 4**)**.

The Sn–Cl bond lengths of the $SnCl_6$ dianion ranged from 2.408(2) Å to 2.431(2)Å. The Cl–Sn–Cl bond angles ranged from 88.64 (5)° to 91.67 (6)° for the chlorine atoms in lateral positions, while those for axial chlorines were close to 180°, exhibiting a small geometrical distortion from the ideal octahedra geometry. The Sn–Cl bonds were in agreement with the corresponding values for similar compounds reported previously [48, 49]. The distance between neighbouring Sn·atoms (Sn….Sn) in the inorganic sheet ranged from 6.923 (2) Å to 7.345 (5) Å. The distortion angle of the metal coordination sphere can be estimated by the calculation of the ∑ parameter [50]. In this study, ∑ was equal to 9.46°, indicative of a weak distortion.

For the two organic chains of $NH_3\text{-}(CH_2)_2\text{-}C_6H_5$ of the unit cell, the carbon atoms exhibited extremely high disorder for the one chain (the equivalent isotropic displacement parameter Ueq values were about 0.102 $Å^2$ and 0.187 $Å^2$), and a slight disorder for the second chain (i.e. Ueq values were about 0.083 $Å^2$ and 0.060 $Å^2$), the values of C–C bond lengths distances were of (1.211 Å and −1.526 Å) and (1.40 Å and −1.50 Å), respectively. The N–C bond lengths were (1.479 Å and 1.482 Å) and C–C–C bond angles ranged from 116° to 125°, respectively. The aromatic ring of the two phenethylaminium cations in the unit cell adopted quite a planar conformation. The torsion angles of N2–C21–C22–C23 and N1–C11–C12–C13 were −174.6° and 178.5°, respectively. The torsion angles of C11–C12–C13–C14, C11–C12–C13–C14, C21–C22–C23–C24 and C21–C22–C23–C28 were −43°, 138.7°, −79° and 102°, respectively, indicating that the ethylaminium group of the two phenethylaminium cations adopts anti-periplanar conformations.

The compound comprised alternating organic and inorganic layers stacked along the *b*-axis. The inorganic layer was formed by isolated octahedras $[SnCl_6]$ **(**Fig. 5**)**. Hydrogen-bond interactions clearly played a key role in the cohesion between layers and stabilized the crystal structure. Indeed, the N–H···Cl hydrogen bond was formed between the two layers, with the NH···Cl distance ranging from 2.686 Å to 2.874 Å. In addition, the CH···Cl hydrogen-bond distance

was about 2.807 Å (Fig. 6).

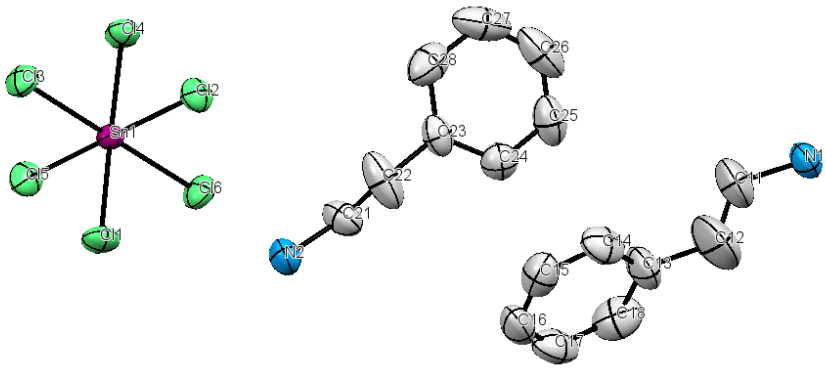

Figure 4: Asymmetric unit cell of organic-inorganic hybrid $(NH_3\text{-}(CH_2)_2\text{-}C_6H_5)_2[SnCl_6]$. hydrogen's atoms are omitted for clarity.

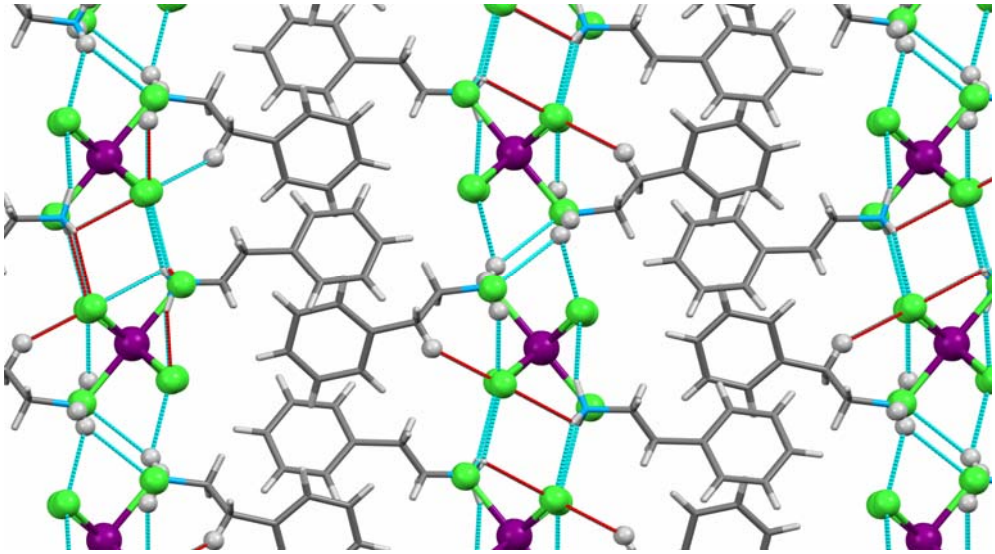

Figure 5: View of the crystal packing projected along the a-axis. The hydrogen bonds are indicated by dashed lines.

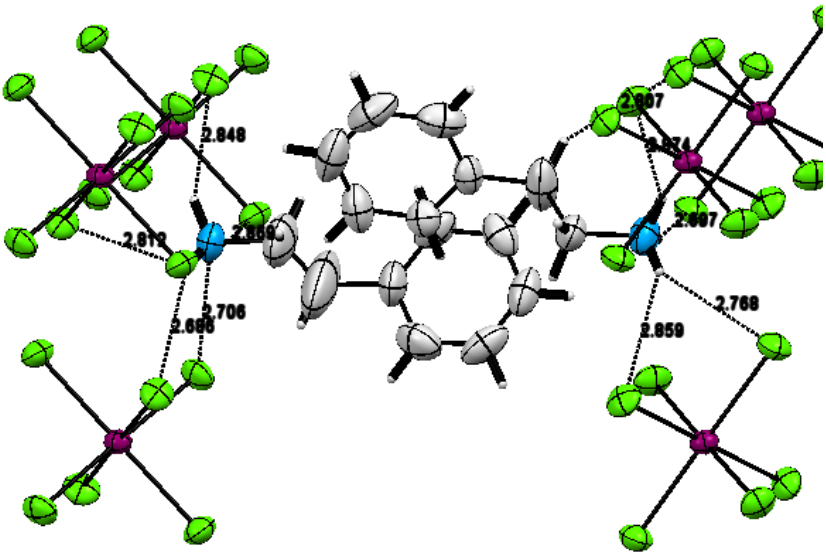

Figure 6: View showing the inter layers' cohesion via N-H…Cl hydrogen bonds (dashed lines).

Fig.7 shows the optimized structure of $(NH_3\text{-}(CH_2)_2\text{-}C_6H_5)_2[SnCl_6]$. The bond lengths and bond angles were in agreement, particularly for $[SnCl_6]^{2-}$ where deviations were between 0.005 Å and 0.273 Å and between 0.6° and 7.7°, respectively. On the other hand, for the organic chain, the deviations were more notably analysed in detail by the calculated geometry, which was related to the torsion angle of the N–C–C–C group. Indeed, in the organic moiety of the examined structure, the C–C bond lengths in the benzene rings for the cations ranged from 1.406 to 1.413 Å. The C–C–C bond angles ranged from 118.9° to 120.7°. These values were within the range of typical values for single and double bonds. The C–C bond lengths of the $^{+}NH_3\text{-}(CH_2)_2$- group ranged from 1.524 Å to 1.546 Å for the two cations, and their N–C bond lengths were 1.513 Å and 1.518 Å. The torsion NCCC for the two chains of the unit cell were about 170.9° and –57.7°, respectively.

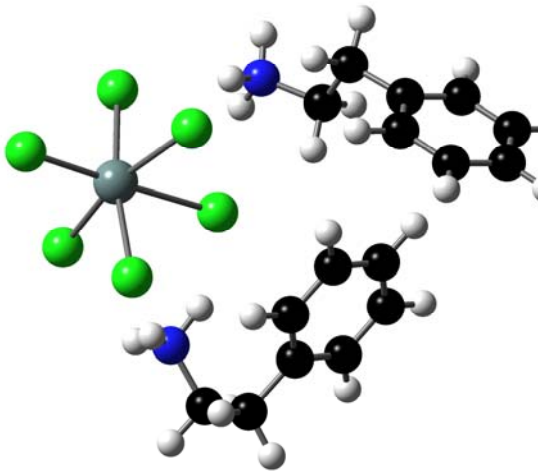

Figure 7: Optimized structure of I calculated by the DFT/B3LYP/LANL2DZ method.

3-5 Hirshfeld Surface

The analysis of intermolecular interactions using the Hirshfeld surface permitted the understanding of interactions in the crystal packing. The Crystal Explorer software was utilized to generate the Hirshfeld surface [37]. Analysis of the intermolecular contacts with an asymmetric unit (Fig8) reveals all of the interlayer interactions calculated by Hirshfeld surfaces d_{norm} mapping. Fig 8a clearly shows all of the contributor contacts on the Hirshfeld surface. Red spots represented the highlighted shorter first type of interactions that are rich in N–H···Cl hydrogen bonds, while the blue and white areas represented the second type of interactions, i.e. H···H, C···H and Cl···Cl. The red regions on the d_{norm} surface were in agreement with the observed interactions in the crystal structure.

The 2D fingerprint plots permitted the highlighting of the contacts of particular atom pairs to separate the contributions from different overlapping interactions in the full fingerprint [1, 51] (Fig 8b). Fig 9 shows the fingerprint plot of the hydrogen-bond contacts. The general H···Cl hydrogen bonds were the most abundant (54.6%) in the crystal packing. The H··· hydrogen bonds constituted 28.4% of the Hirshfeld surface, corresponding to the second-most frequent contacts due to the presence of hydrogen atoms on the molecular surface. The Cl··· long interatomic interactions constituted 3.7% in the centre of the 2D fingerprint maps, while the C···H contacts represented 13.2% of the total Hirshfeld surface (aromatic ring). From a quantitative viewpoint, H···Cl contacts were clearly the most abundant contacts in the structure, and they ensured the cohesion of crystal packing. Table 2 summarizes the ratio of their contributions.

Hirshfeld surface analysis is crucial and promising in crystal engineering because it permits quantitative and qualitative analyses by indicating all hydrogen-bond interactions.

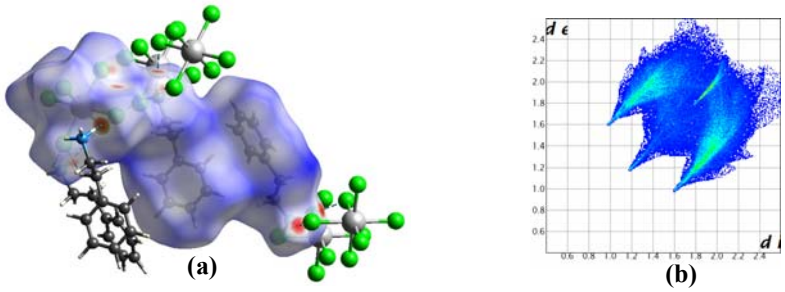

Figure 8: Hirshfeld Surfaces mapped with dnorm for the title compound.

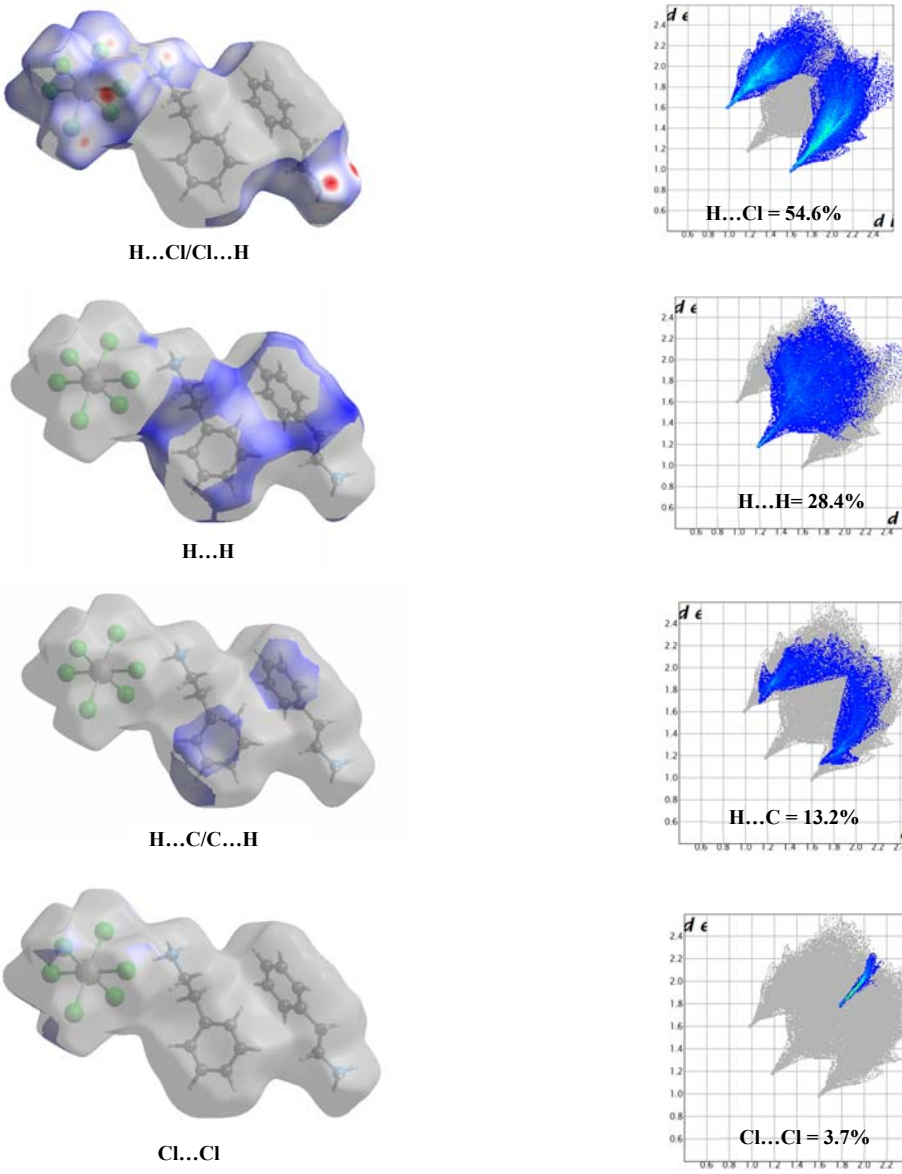

Figure 9: 2D fingerprint plot (99.9%) of $(NH_3\text{-}(CH_2)_2\text{-}C_6H_5)_2[SnCl_6]$, showing contributions from different contacts.

Table 2: Summary of the major short contacts and their contribution percentage to the Hirshfeld surface.

Type of contact	Contribution (%)
H···Cl/Cl…H	54.6
H···H	28.4
H···C/ C···H	13.2
Cl···Cl	3.7

3-6 Raman spectroscopy of $(NH_3\text{-}(CH_2)_2\text{-}C_6H_5)_2[SnCl_6]$.

To obtain more information about the titled compound structure, vibrational modes in the range of 400 and 4500 cm^{-1} were examined by Raman spectroscopy. To obtain further insights into the structure, Raman spectra were recorded using a green laser at λ = 532 nm and different powers in the range of 0.25 to 25 mW (Fig 10). Clearly, the peak intensity varied depending on the power. A more resolved spectrum was obtained at P = 6.25 mW. Indeed, the spectra were divided in intervals, i.e. in a low-frequency range of 50–400 cm^{-1} and a high-frequency range of 400–4250 cm^{-1}.

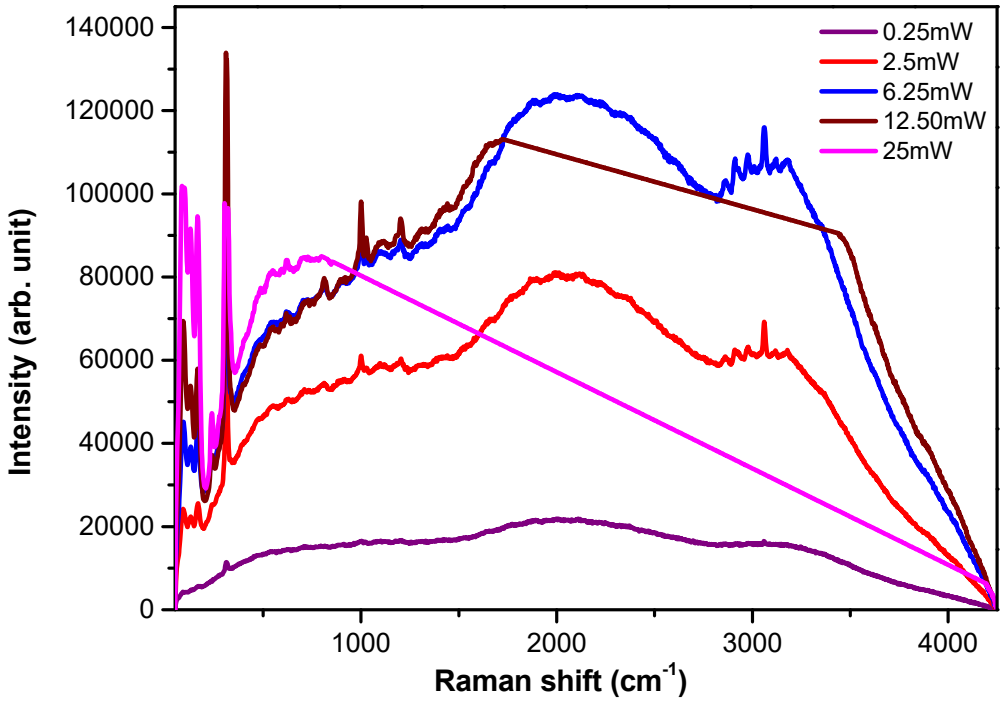

Figure 10. Raman spectrum of $(NH_3\text{-}(CH_2)_2\text{-}C_6H_5)_2[SnCl_6]$, using a green laser at 532 nm and at P = 0.25, 2.5, 6.25, 12.50 and 25 mW

For the low frequency shown in Fig 11, by referring and essentially comparing with a number of hexachloridostannate(IV) compounds in previous studies [1, 48, 52, 53], all vibrational bands corresponding to $(SnCl_6)^{2-}$ were observed at less than 350 cm^{-1}. An intense band observed at 311 cm^{-1} corresponded to the asymmetric stretching vibrations of υ_a(Sn–Cl). The shoulder band observed at 236 cm^{-1} corresponded to the symmetric stretching

vibrations of ν_s(Sn–Cl)). The bands observed at 91 and 165 cm^{-1} corresponded to the symmetric and asymmetric bending vibrations of Cl–Sn–Cl, respectively.

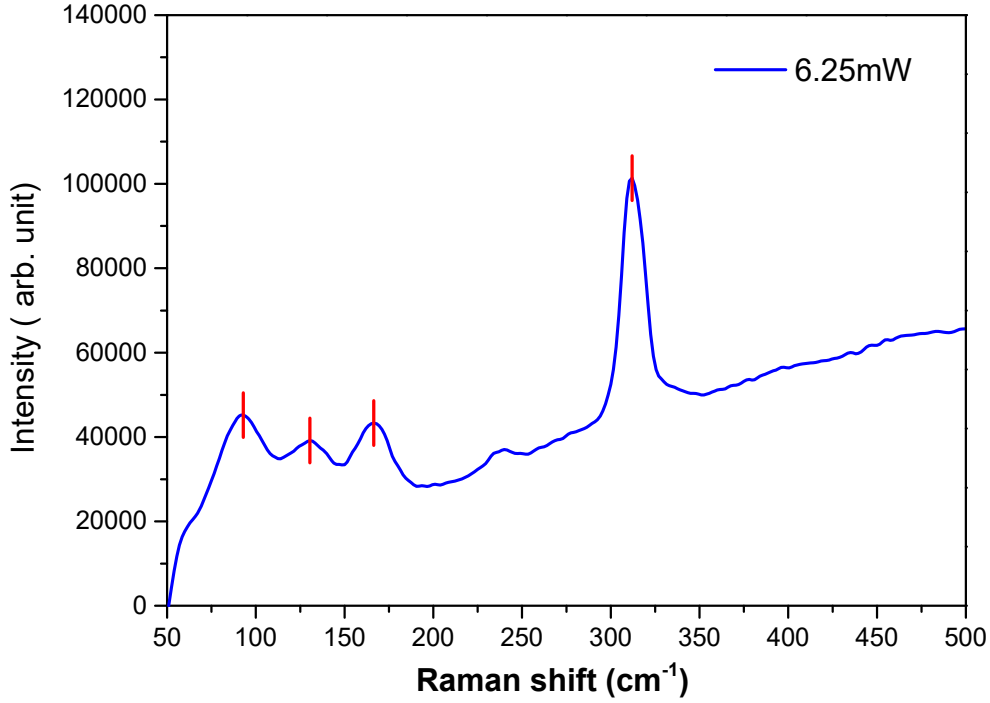

Figure11. Raman spectrum of $(NH_3\text{-}(CH_2)_2\text{-}C_6H_5)_2[SnCl_6]$ in the range of 50–500 cm^{-1} using a green laser at 532 nm at P = 6.25 mW

In the high-frequency region shown in Fig 12, stretching vibrations of the NH_3^+ group were observed at υ_s = 3053 cm^{-1} and υ_a = 3118 cm^{-1}, which was interconnected by a system of hydrogen bonds in the (N–H···Cl) crystal [54-56]. Symmetric and asymmetric stretching vibrations of (-CH_2-) were observed between 2800 and 3000 cm^{-1}. In- and out-of-plane deformation bands of the aromatic rings were observed at 706 and 806 cm^{-1}, respectively. The C–C and C–N stretching modes were observed at 911 and 1007 cm^{-1}, respectively, while the rocking vibration of the NH_3 group was detected at 1209 cm^{-1}.

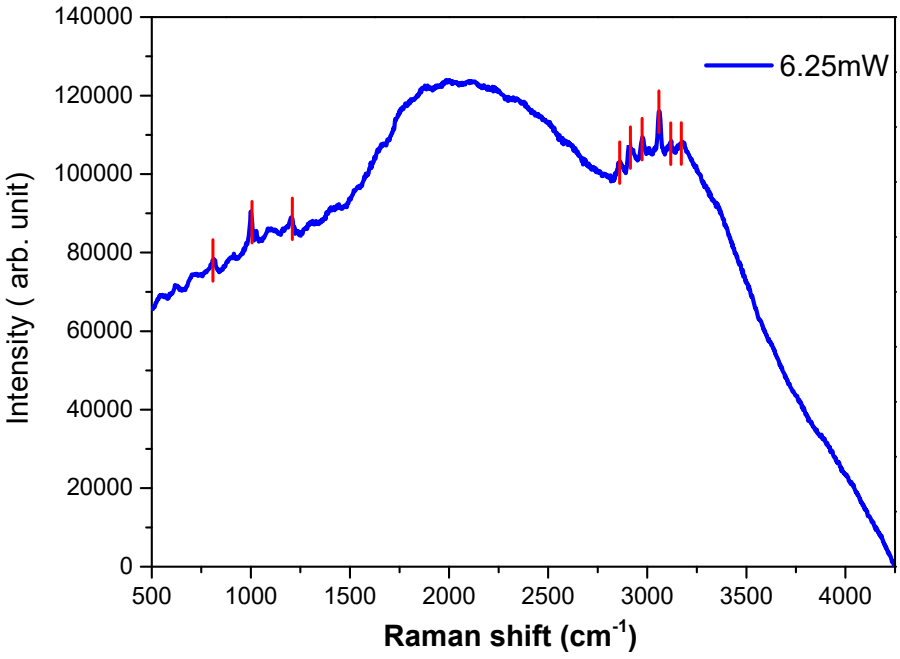

Figure12. Raman spectrum of $(NH_3\text{-}(CH_2)_2\text{-}C_6H_5)_2[SnCl_6]$ in the range of 500–4250 cm^{-1} using a green laser of 532 nm at P = 6.25 mW

To assign the Raman bands, the spectrum was calculated. Experimental and theoretical values calculated from the band positions were in extremely good agreement, permitting the unambiguous assignment of the different Raman signals as shown in Figure 13.

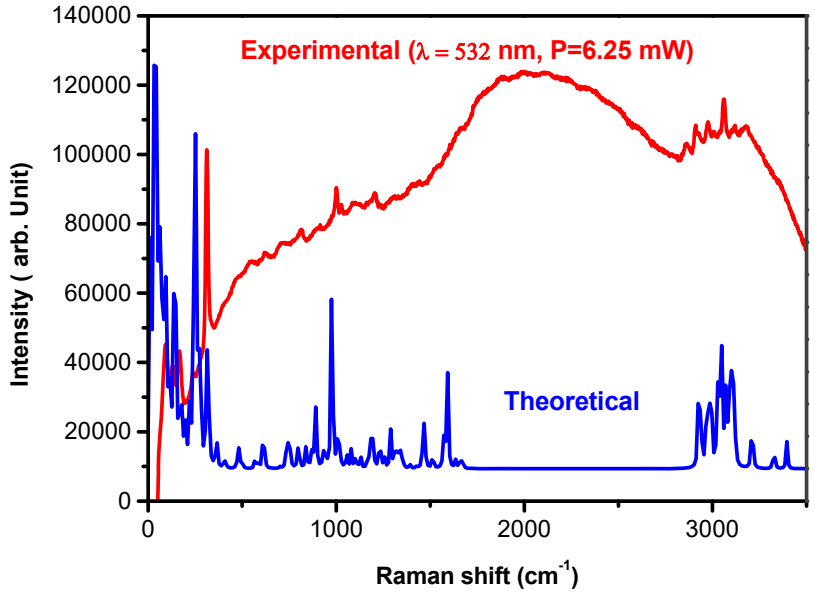

Figure 13: Calculated and experimental Raman spectrum of $(NH_3\text{-}(CH_2)_2\text{-}C_6H_5)_2[SnCl_6]$.

3-7 Antibacterial activity

The antibacterial activity of the synthesized compound was evaluated against two gram-negative bacteria, viz. *Escherichia coli* (EC) and *Pseudomonas aeruginosa* (PA), respectively, and two gram-positive bacteria, viz. *Bacillus subtilis* (BS) and *Methicillin-resistant Staphylococcus aureus* (MRSA), respectively, in terms of MIC [57]. Table 3 summarizes the results.

The as-synthesized compound $(NH_3\text{-}(CH_2)_2\text{-}C_6H_5)_2[SnCl_6]$ was active against all bacteria strains, with MIC values comparable to those obtained by using standard antibiotic ciprofloxacin as a reference (Table 3).

Table 3. Antibacterial activity of $(NH_3\text{-}(CH_2)_2\text{-}C_6H_5)_2[SnCl_6]$.

Derivative	**Bacteria** MIC (µg/mL)			
	EC	***PA***	***BS***	***MRSA***
Prepared compound	12.5	12.5	25	25
Ciprofloxacin	12.5	12.5	12.5	18.75

[a]MIC in µg/mL.

In addition, morphological changes of the microorganisms by the as-synthesized compound were analysed by SEM. Fig 14 shows the SEM images of untreated bacteria with a regular rod shape. In contrast, after treatment, bacteria were not visible. Thus, serious damage of the microorganisms is observed.

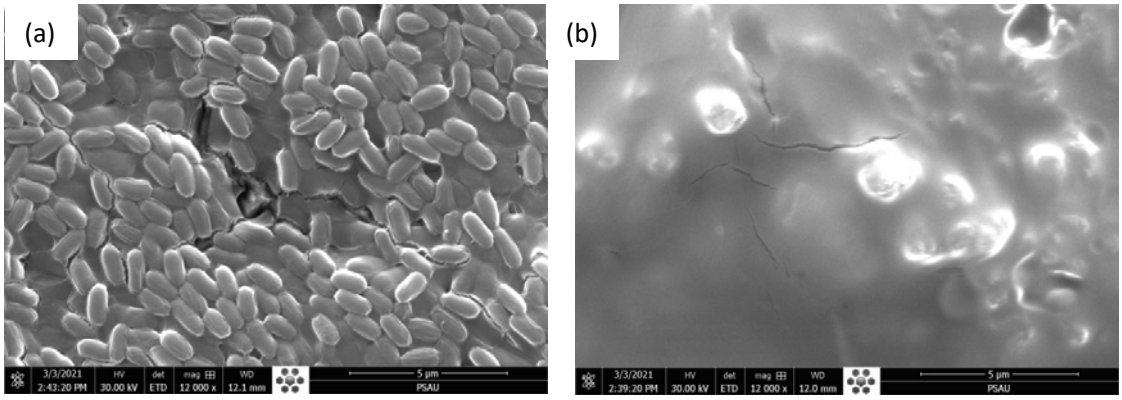

Figure 14. SEM images of K. pneumoniae (a) before treatment and (b) after treatment.

4- Conclusion

In the summery, the synthesis and characterization of a new single crystal of an organic inorganic hybrid compound (Phenethylaminium) hexachlorostannate In summary, the synthesis and characterization of a new single crystal of an organic–inorganic hybrid compound (phenethylaminium) hexachlorostannate are reported. In addition, its structure is characterized and confirmed by SEM, Raman spectroscopy and XRD. The optimization and assignment of the vibrational modes are calculated by the DFT/B3LYP/LANL2DZ method to obtain clear insights into the examined

compound. The compound exhibits an ionic structure, comprising alternating organic and inorganic sheets in the form of a layered perovskite system. 3D Hirshfeld surface analysis reveals that the cohesion and stabilization of the structure predominantly occurs due to H···Cl and H···H hydrogen-bond interactions. The synthesized compound $(NH_3\text{-}(CH_2)_2\text{-}C_6H_5)_2[SnCl_6]$ was highly active against Escherichia coli (EC) and Pseudomonas aeruginosa (PA), while a medium effect was obtained on the rest of the studied bacterial strains.

References

[1] S. BelhajSalah, M.S. Abdelbaky, S. García-Granda, K. Essalah, C.B. Nasr, M. Mrad, Crystal structure, Hirshfeld surfaces computational study and physicochemical characterization of the hybrid material (C7H10N) 2 [SnCl6]· H2O, Journal of Molecular Structure 1152 (2018) 276-286.

[2] M.H. Mrad, I. Feddaoui, M.S. Abdelbaky, S. García-Granda, C.B. Nasr, Elaboration, crystal structure, characterization and DFT calculation of a new Hg (II) inorganic-organic hybrid salt [C6H16N2O] HgCl4, Journal of Solid State Chemistry (2020) 121280.

[3] C. Bejaoui, I. Ameur, N. Derbel, A. Linden, S. Abid, DFT calculations, crystal structure, Hirshfeld surface analyses and antibacterial studies of a new tetrachlorocuprate salt:(C6H16N2O)[CuCl4], Journal of Molecular Structure 1166 (2018) 7-14.

[4] S. Bouacida, R. Bouchene, F. Berrah, Synthesis, crystal structure, hirshfeld surface analysis, DFT calculations and thermal properties of a new anilinium derivative chlorostannate (IV) hybrid compound, Journal of Molecular Structure 1198 (2019) 126900.

[5] I. Feddaoui, M.S. Abdelbaky, S. García-Granda, K. Essalah, C.B. Nasr, M. Mrad, Synthesis, crystal structure, vibrational spectroscopy, DFT, optical study and thermal analysis of a new stannate (IV) complex based on 2-ethyl-6-methylanilinium (C9H14N) 2 [SnCl6], Journal of Molecular Structure 1186 (2019) 31-38.

[6] O.B. Moussa, H. Chebbi, Y. Arfaoui, L.R. Falvello, M. Tomas, M.F. Zid, Structural study, vibrational and optical properties, Hirshfeld surface analysis and DFT investigation of a novel organic cation hexachloridostannate (IV),(C5H8N3) 2 [SnCl6], Journal of Molecular Structure 1195 (2019) 344-354.

[7] D.B. Mitzi, K. Chondroudis, C.R. Kagan, Organic-inorganic electronics, IBM journal of research and development 45 (2001) 29-45.

[8] N.L. Allan, M.J. Dayer, D.T. Kulp, W.C. Mackrodt, Atomistic lattice simulations of the ternary fluorides AMF3 (A= Li, Na, K, Rb, Cs; M= Mg, Ca, Sr, Ba), Journal of Materials Chemistry 1 (1991) 1035-1039.

[9] G.C. Papavassiliou, Three-and low-dimensional inorganic semiconductors, Progress in Solid State Chemistry 25 (1997) 125-270.

[10] A. Lemmerer, D.G. Billing, Synthesis, characterization and phase transitions of the inorganic–organic layered perovskite-type hybrids [(C n H 2n+ 1 NH 3) 2 PbI 4], n= 7, 8, 9 and 10, Dalton Transactions 41 (2012) 1146-1157.

[11] H. Abid, A. Trigui, A. Mlayah, E. Hlil, Y. Abid, Phase transition in organic–inorganic perovskite (C9H19NH3) 2 PbI2Br2 of long-chain alkylammonium, Results in Physics 2 (2012) 71-76.

[12] P. Vaněk, M. Havrankova, J. Hybler, Phase transitions in (CH3) 4NPbBr3, Solid state communications 82 (1992) 509-512.

[13] D.B. Mitzi, P. Brock, Structure and optical properties of several organic− inorganic hybrids containing corner-sharing chains of bismuth iodide octahedra, Inorganic chemistry 40 (2001) 2096-2104.

[14] A.M. Leguy, Y. Hu, M. Campoy-Quiles, M.I. Alonso, O.J. Weber, P. Azarhoosh, M. Van Schilfgaarde, M.T. Weller, T. Bein, J. Nelson, Reversible hydration of CH3NH3PbI3 in films, single crystals, and solar cells, Chemistry of Materials 27 (2015) 3397-3407.

[15] Y. Dang, Y. Liu, Y. Sun, D. Yuan, X. Liu, W. Lu, G. Liu, H. Xia, X. Tao, Bulk crystal growth of hybrid perovskite material CH 3 NH 3 PbI 3, CrystEngComm 17 (2015) 665-670.

[16] J.H. Heo, S.H. Im, J.H. Noh, T.N. Mandal, C.-S. Lim, J.A. Chang, Y.H. Lee, H.-j. Kim, A. Sarkar, M.K. Nazeeruddin, Efficient inorganic–organic hybrid heterojunction solar cells containing perovskite compound and polymeric hole conductors, Nature photonics 7 (2013) 486.

[17] R. Liu, Hybrid organic/inorganic nanocomposites for photovoltaic cells, Materials 7 (2014) 2747-2771.

[18] Y. Zhao, K. Zhu, Efficient planar perovskite solar cells based on 1.8 eV band gap CH3NH3PbI2Br nanosheets via thermal decomposition, Journal of the American Chemical Society 136 (2014) 12241-12244.
[19] G. Peng, X. Xu, G. Xu, Hybrid organic-inorganic perovskites open a new era for low-cost, high efficiency solar cells, Journal of Nanomaterials 2015 (2015).
[20] G.V. Prakash, K. Pradeesh, R. Ratnani, K. Saraswat, M. Light, J. Baumberg, Structural and optical studies of local disorder sensitivity in natural organic–inorganic self-assembled semiconductors, Journal of Physics D: Applied Physics 42 (2009) 185405.
[21] C. Aruta, F. Licci, A. Zappettini, F. Bolzoni, F. Rastelli, P. Ferro, T. Besagni, Growth and optical, magnetic and transport properties of (C 4 H 9 NH 3) 2 MCl 4 organic-inorganic hybrid films (M= Cu, Sn), Applied Physics A 81 (2005) 963-968.
[22] C. Kagan, D. Mitzi, C. Dimitrakopoulos, Organic-inorganic hybrid materials as semiconducting channels in thin-film field-effect transistors, Science 286 (1999) 945-947.
[23] J.L. Knutson, J.D. Martin, D.B. Mitzi, Tuning the band gap in hybrid tin iodide perovskite semiconductors using structural templating, Inorganic chemistry 44 (2005) 4699-4705.
[24] P. Chandrasekhar, B.J. Zay, G.C. Birur, S. Rawal, E.A. Pierson, L. Kauder, T. Swanson, Large, Switchable Electrochromism in the Visible Through Far-Infrared in Conducting Polymer Devices, Advanced Functional Materials 12 (2002) 95-103.
[25] Y. Li, S. Innocentin, D.R. Withers, N.A. Roberts, A.R. Gallagher, E.F. Grigorieva, C. Wilhelm, M. Veldhoen, Exogenous stimuli maintain intraepithelial lymphocytes via aryl hydrocarbon receptor activation, Cell 147 (2011) 629-640.
[26] G. Matela, R. Aman, C. Sharma, S. Chaudhary, Reactions of tin-and triorganotin (IV) isopropoxides with thymol derivative: synthesis, characterization and in vitro antimicrobial screening, Journal of the Serbian Chemical Society 78 (2013) 1323-1333.
[27] M. Nath, P.K. Saini, Chemistry and applications of organotin (IV) complexes of Schiff bases, Dalton Transactions 40 (2011) 7077-7121.
[28] M. Mathlouthi, A. Valkonen, M. Rzaigui, W. Smirani, Structural characterization, spectroscopic, thermal, AC conductivity and dielectric properties and antimicrobial studies of (C8H12N) 2 [SnCl6], Phase Transitions 90 (2017) 399-414.
[29] E.J. Mittemeijer, U. Welzel, Modern diffraction methods, John Wiley & Sons2013.
[30] A. Altomare, M.C. Burla, M. Camalli, G.L. Cascarano, C. Giacovazzo, A. Guagliardi, A.G. Moliterni, G. Polidori, R. Spagna, SIR97: a new tool for crystal structure determination and refinement, Journal of Applied Crystallography 32 (1999) 115-119.
[31] S. GM, SHELX-97, release 97-2, University of Göttingen, Germany (1998).
[32] L.J. Farrugia, WinGX suite for small-molecule single-crystal crystallography, Journal of Applied Crystallography 32 (1999) 837-838.
[33] K. Brandenburg, DIAMOND 3.1 a., version 1.1 a, Crystal Impact GbR, Bonn, Germany 2005 (1997).
[34] C.F. Macrae, I.J. Bruno, J.A. Chisholm, P.R. Edgington, P. McCabe, E. Pidcock, L. Rodriguez-Monge, R. Taylor, J. Streek, P.A. Wood, Mercury CSD 2.0–new features for the visualization and investigation of crystal structures, Journal of Applied Crystallography 41 (2008) 466-470.
[35] D.G. Billing, A. Lemmerer, M.J.A.C.S.C.C.S.C. Rademeyer, Bis (1-phenylethylammonium) hexachloridostannate (IV) and bis (2-phenylethylammonium) hexachloridostannate (IV), 63 (2007) m101-m104.
[36] J.J. McKinnon, D. Jayatilaka, M.A.J.C.C. Spackman, Towards quantitative analysis of intermolecular interactions with Hirshfeld surfaces, (2007) 3814-3816.
[37] M. Turner, J. McKinnon, S. Wolff, D. Grimwood, P. Spackman, D. Jayatilaka, M. Spackman, CrystalExplorer. Version 17. University of Western Australia, 2017.
[38] M. Frisch, G. Trucks, H. Schlegel, G. Scuseria, M. Robb, J. Cheeseman, G. Scalmani, V. Barone, G. Petersson, H. Nakatsuji, Gaussian 16, revision C. 01. Wallingford: Gaussian, Inc, 2016.
[39] A. Becke, Density-functional thermochemistry. III. The role of exact exchange (1993) J, Chem. Phys 98 5648.
[40] R. Parr, W. Yang, Density functional theory of atoms and moleculesoxford univ, Press, New York (1989).
[41] C. Lee, W. Yang, R.G. Parr, Development of the Colle-Salvetti correlation-energy formula into a functional of the electron density, Physical review B 37 (1988) 785.
[42] P.J. Stephens, F.J. Devlin, C.F. Chabalowski, M.J. Frisch, Ab initio calculation of vibrational absorption and circular dichroism spectra using density functional force fields, The Journal of physical chemistry 98 (1994) 11623-11627.

[43] P.J. Hay, W.R. Wadt, Ab initio effective core potentials for molecular calculations. Potentials for the transition metal atoms Sc to Hg, The Journal of chemical physics 82 (1985) 270-283.
[44] R.D. Johnson, NIST computational chemistry comparison and benchmark database, http://srdata. nist. gov/cccbdb (2006).
[45] R. Dennington, T. Keith, J. Millam, GaussView, version 5, (2009).
[46] K. Elmebrouki, S. Tamsamani, M. Khechoubi, Synthesis and characterization of new materials like perovskite [NH3-(CH2) n-NH3] ZnCl4 avec n= 8 et 10, Journal of Asian Scientific Research 1 (2011) 216.
[47] M. Saber Lassoued, W. Ben Soltan, M.S. Abdelbaky, S. Ammar, A. Gadri, A. Ben Salah, S. García-Granda, Structural, vibrational and optical properties of a new self-assembled organic-inorganic crystal (C4H7N2)[CdCl3 (H2O)], (2017).
[48] S. Bouacida, H. Kechout, R. Belhouas, H. Merazig, T. Roisnel, Bis (3-hydroxymethylanilinium) hexachloridostannate (IV), Acta Crystallographica Section E: Structure Reports Online 67 (2011) m395-m395.
[49] R. Rouchene, Z. Lecheheb, R. Relhouas, S. Bouacida, Synthesis, X-ray diffraction and Hirshfeld surface analysis of two new hybrid dihydrate compounds:(C6H22N4)[SnCl6] Cl-2 center dot 2H (2) O and (C8H24N4)[SnCl6] Cl-2 center dot 2H (2) O, ACTA CRYSTALLOGRAPHICA SECTION E-CRYSTALLOGRAPHIC COMMUNICATIONS 74 (2018) 206-+.
[50] P. Guionneau, Crystallography and spin-crossover. A view of breathing materials, Dalton Transactions 43 (2014) 382-393.
[51] I. Mkaouar, N. Karâa, B. Hamdi, R. Zouari, Synthesis, crystal structure, thermal analysis, vibrational study dielectric behaviour and Hirshfeld surface analysis of [C6H10 (NH3) 2)] 2 SnCl6 (Cl) 2, Journal of Molecular Structure 1115 (2016) 161-170.
[52] M. Daszkiewicz, M.K. Marchewka, Crystal structure, vibrational and theoretical studies of bis (4-amino-1, 2, 4-triazolium) hexachloridostannate (IV), Journal of Molecular Structure 1017 (2012) 90-97.
[53] M.S. Lassoued, M.S. Abdelbaky, R.M. Meroño, A. Gadri, S. Ammar, A.B. Salah, S. García-Granda, Structure, spectroscopic measurement, thermal studies and optical properties of a new hybrid compound of aquapentachloroindoidate (III) complex, Journal of Molecular Structure 1142 (2017) 73-79.
[54] S. Gatfaoui, A. Mezni, T. Roisnel, H. Marouani, Synthesis, characterization, Hirshfeld surface analysis and antioxidant activity of a novel organic-inorganic hybrid material 1-methylpiperazine-1, 4-diium bis (nitrate), Journal of Molecular Structure 1139 (2017) 52-59.
[55] S. Soudani, M. Zeller, C. Jelsch, F. Lefebvre, C.B. Nasr, Structural, Hirshfeld surface and spectroscopic studies of the noncentrosymmetric 1-ethylpiperazinediium pentachloroantimonate (III) monohydrate, Solid State Sciences 58 (2016) 94-100.
[56] S. Kassou, A. Kaiba, P. Guionneau, A. Belaaraj, Organic-inorganic hybrid perovskite (C 6 H 5 (CH 2) 2 NH 3) 2 CdCl 4: Synthesis, structural and thermal properties, Journal of Structural Chemistry 57 (2016) 737-743.
[57] I. Wiegand, K. Hilpert, R.E. Hancock, Agar and broth dilution methods to determine the minimal inhibitory concentration (MIC) of antimicrobial substances, Nature protocols 3 (2008) 163.